Coupled electron–hole quantum well structure: mass asymmetry and finite width effects

2006 J. Phys.: Condens. Matter 18 1285

(http://iopscience.iop.org/0953-8984/18/4/014)

INSTITUTE OF PHYSICS PUBLISHING JOURNAL OF PHYSICS: CONDENSED MATTER

J. Phys.: Condens. Matter **18** (2006) 1285–1301 doi:10.1088/0953-8984/18/4/014

Coupled electron–hole quantum well structure: mass asymmetry and finite width effects

R K Moudgil

Department of Physics, Kurukshetra University, Kurukshetra-136 119, India

E-mail: rkmoudgil13@rediffmail.com

Received 31 May 2005
Published 11 January 2006
Online at stacks.iop.org/JPhysCM/18/1285

Abstract

We investigate the role of many-body correlations in determining the ground-state behaviour of the coupled electron–hole quantum well structure by including the mass asymmetry and the finite width of wells. The correlations (both the intra- and inter-well) are treated beyond the static local-field theories by employing the dynamical self-consistent mean-field approximation of Hasegawa and Shimizu. The mass asymmetry is seen to introduce a marked change in the ground state of the electron–hole system as compared to the recent corresponding results on the mass-symmetric electron–hole bilayer. First, the critical density for the liquid–Wigner crystal phase transition is greatly enhanced (e.g., by a factor of about 4 for a GaAs/GaAlAs based system). Second, there is a change in the role played by the electron–hole correlations. The Wigner crystal phase is now found to be stable below a critical density only at sufficiently large separation between the wells. The build-up of electron–hole correlations with diminishing inter-well spacing tends to favour the charge-density-wave phase over the Wigner crystal state, with the result that the former always prevails in the sufficiently close approach of wells. This result differs strikingly from the corresponding studies on the mass-symmetric system, since the electron–hole correlations are predicted here to always support, at sufficiently small well spacing, the Wigner crystal phase below a critical density and the charge-density-wave phase at relatively higher densities. Further, we find that the inclusion of the finite width of layers results in lowering of the critical density for Wigner crystallization.

1. Introduction

Electron–hole (e–h) systems have been drawing a lot of interest over the years [1]. The early studies focused on systems such as those realized in the bulk semiconductors [2], where electrons and holes occupy the same region in space. However, the recent progress in nanoscale semiconductor fabrication technology has made it possible to have e–h systems in coupled

semiconductor quantum well structures [3]; here, electrons and holes are confined quantum mechanically in two adjacent quantum wells, which are separated in real space. Such e–h systems have proved relatively advantageous over those in conventional bulk semiconductors not only since the electrons and holes are spatially separated here, but also due to having a direct control on the carrier number density and the inter-well spacing, and hence, on the strength of carrier interactions. Due to these reasons, this class of e–h systems has attracted considerable attention in recent years and many interesting phenomena have been discovered. Notably, the existence of an excitonic condensate phase, which was postulated many years ago [4], has been confirmed experimentally [5] in these systems. On the other hand, the recent theoretical investigations [6–9] on coupled layers of electrons and holes have predicted, apart from the possibility of the excitonic phase, the stability of a density-modulated (DM) ground state in the close vicinity of two layers. More precisely, two types of DM phase have been predicted: the Wigner crystal (WC) phase below a critical density and the charge-density-wave (CDW) phase at relatively higher densities. As an important finding [6, 9], the critical density for Wigner crystallization has been found to be significantly higher than the corresponding value for an isolated single layer. The prediction on the enhancement of Wigner crystallization has been confirmed by the recent diffusion Monte Carlo simulations due to De Palo *et al* [10].

In the present work, we are primarily concerned with the e–h system as realized in a coupled quantum well structure. We wish to examine the role of many-body correlations in determining the ground-state behaviour of such a system. Earlier, Zheng and MacDonald [11], Szymanski *et al* [6] and Liu *et al* [7] have studied the correlation effects on the basis of a generalized mean-field approximation. Alatalo *et al* [12] have used the multicomponent hypernetted-chain method to treat the correlations and have also extended their calculation to a related system of more than two layers. The intra- and inter-layer correlations were treated in [7] and [11] by using the Singwi, Tosi, Land and Sjölander (STLS) [13] approach. However, Szymanski *et al* [6] argued that the STLS approach could not be applicable at densities down to Wigner crystallization (i.e., in the strongly correlated regime) and, thereby, proposed a different method for incorporating correlations in these situations: correlations within the layers were included in the form of an STLS-like local-field correction (LFC) and the required static structure factor was taken from the Monte Carlo simulation data of Tanatar and Ceperley [14], while the correlations between the layers were treated within the STLS approach. This calculation revealed that the e–h liquid could become unstable, at sufficiently small layer separation, with respect to a DM ground state of the CDW and WC types. The WC phase dominated at densities $r_s \geqslant 15$, and the CDW phase for $r_s < 15$. Here, $r_s = 1/(a_0^*\sqrt{n\pi})$ is a dimensionless density parameter with n being the areal density of carriers in either of the layers and a_0^* the effective Bohr atomic radius. On the other hand, the conventional STLS approach predicted [7, 8] always an instability towards a CDW ground state. In a recent work, Moudgil *et al* [9] have considered correlations beyond the static local-field theories by extending the dynamical self-consistent mean-field approximation of Hasegawa and Shimizu [15] (the so-called quantum or dynamical STLS approach) to the bilayer system. It was found that the dynamical STLS approach provided on the whole a better description of correlations than the conventional STLS method as adjudged by a direct comparison with the computer simulation experiments [10]. Further, the dynamical STLS approach accounted in a natural way for the transition to both the CDW and WC phases. The WC phase was predicted to be stable for $r_s \geqslant 10$, and the CDW phase for $r_s < 10$.

However, in all of the above mentioned theoretical as well as simulation studies, the holes were assumed to have the same effective mass as the electrons, but this is not so in a real physical situation; for instance, $m_h^*/m_e^* \approx 7$ for a GaAs/GaAlAs based e–h system. m_h^* (m_e^*) denotes the effective mass of holes (electrons). The mass asymmetry between the electron

and hole layers should make, at the same number density of carriers, the (heavier) holes comparatively more correlated than the electrons, and it may influence the overall ground-state behaviour of the e–h system. Our present study is partly motivated by this gap between the theory and the actual physical scenario. We intend to examine in this paper the ground-state behaviour of the coupled e–h system by including the mass asymmetry of electrons and holes. To be even more close to reality, we also plan to include in our study the finite thickness of the electron and hole layers. We will treat the intra- and inter-layer correlations at the same level of approximation within the tested dynamical STLS [15] approach. It is appropriate to point out here that Alatalo *et al* [16] have earlier studied the effect of finite thickness of layers by employing the variational hypernetted-chain approach for correlations. Recently, Kainth *et al* [17] have examined the impact of finite width on the excitation spectrum of an electron bilayer.

The paper is organized as follows. In section 2, we give the model used to represent the coupled e–h quantum well structure. The theoretical formalism is developed here. Section 3 contains results and discussion on the correlation functions, with particular emphasis on the question of the existence of liquid-DM phase transition in a GaAs/GaAlAs based e–h system. The concluding remarks are given in section 4.

2. Bilayer model and theoretical formalism

2.1. Bilayer model

Consider a double-quantum-well structure as realized in a system consisting of two coupled units of a semiconductor heterostructure, e.g., a GaAs/GaAlAs/GaAs heterostructure. In the e–h quantum well system, electrons and holes are the respective carriers in the two wells. The wells are assumed to be identical in each respect except for the charge and mass of holes. In both the wells, the motion of carriers is free along the plane of semiconductor layer (say, the xy-plane), while it is restricted quantum-mechanically in the transverse direction (i.e., the z-direction) due to a finite potential barrier in this direction. Accordingly, the single-particle energies and their corresponding wavefunctions in the well l (l = e or h, is the well index) are given, respectively, by

$$\mathcal{E}_l = \frac{\hbar^2 K^2}{2m_l^*} + \mathcal{E}_{l,z} \tag{1}$$

and

$$\phi_l(\mathbf{R}, z) = A\mathrm{e}^{\mathrm{i}\mathbf{K}\cdot\mathbf{R}}\zeta_l(z), \tag{2}$$

where m_l^* is the effective mass of carriers in the lth well, $\mathcal{E}_{l,z}$ represents the energy of z-motion with $\zeta_l(z)$ as the corresponding wavefunction and A is the appropriate normalization constant. It may be noticed that capital letters have been used to denote the in-plane quantities. The quasi-continuous values of in-plane energy combined with the discrete set of values of $\mathcal{E}_{l,z}$ give rise to the formation of well-known energy sub-bands. At zero temperature, which is the case considered here, we assume that the carriers in both the wells occupy only the lowest energy sub-band.

On considering the finite extension of $\zeta_l(z)$ in the z-direction, the interaction potential between carriers in the wells l and l' is given by

$$V_{ll'}(R) = \alpha_{ll'}\frac{e^2}{\epsilon_0}\int \mathrm{d}z \int \mathrm{d}z' \frac{|\zeta_l(z)|^2|\zeta_{l'}(z')|^2}{\sqrt{R^2 + (z'-z)^2}}, \tag{3}$$

or its Fourier transform by $V_{ll'}(Q) = \alpha_{ll'} V(Q) F_{ll'}(Q)$, where $V(Q) = 2\pi e^2/(Q\epsilon_0)$ and $F_{ll'}(Q)$, which is commonly referred to as the form factor, is given by

$$F_{ll'}(Q) = \int \mathrm{d}z \int \mathrm{d}z' \mathrm{e}^{-Q|z'-z|} |\zeta_l(z)|^2 |\zeta_{l'}(z')|^2. \tag{4}$$

Here, ϵ_0 is the dielectric constant of the background material, and $\alpha_{ll'}$ equals $+1$ for $l = l'$ and -1 otherwise. $F_{ll'}(Q)$ can be determined from the knowledge of the solution of the single-particle Schrödinger equation

$$\left[\frac{-\hbar^2}{2m_l^*}\frac{\mathrm{d}^2}{\mathrm{d}z^2} + V_l(z)\right]\zeta_l(z) = \mathcal{E}_{l,z}\zeta_l(z), \tag{5}$$

for the z-motion. $V_l(z)$ is obviously the (effective) potential energy function for the z-motion. It includes, apart from the Hartree term, the effect of exchange-correlations and this fact alone makes the solution of equation (5), and hence the calculation of $F_{ll'}(Q)$, an extremely complex problem.

Equation (5) has been solved numerically by many researchers (see, for example, reference [18]) starting with different approximate choices for the effective potential $V_l(z)$. The exact behaviour of the form factor will depend in general upon the details regarding geometry of the quantum wells in a particular experiment [17, 19]. However, to illustrate the role of the finite width of layers, we use here the model of Fang and Howard [18, 20]. In this model, the authors have fitted variationally their numerical results to a simple analytical wavefunction, $\zeta_l(z) = (b^3/2)^{1/2} z \exp(-bz/2)$ and the variational parameter b is given for the lowest energy sub-band by $b = (33\pi m_l^* e^2 n/(2\epsilon_0\hbar^2))^{1/3}$. Within the above model, the in-layer form factor $F_{ll}(Q)$ is given by

$$F_{ll}(Q) = \left(1 + \frac{Q}{b}\right)^{-3}\left[1 + \frac{9}{8}\frac{Q}{b} + \frac{3}{8}\left(\frac{Q}{b}\right)^2\right]. \tag{6}$$

For the inter-layer interaction, we continue to ignore the effect of finite width of layers with the belief that it will be small at sufficiently large spacings. Accordingly, we take in our model $V_{\mathrm{eh}}(Q) = -V(Q)\exp(-Qd)$, where d may now be regarded as the average inter-layer spacing, i.e., the distance between the means of the carrier envelope function $|\zeta_l(z)|^2$ in the two wells. Further, we assume that the layers are sufficiently apart so as to preclude the possibility of tunnelling across the layers. Thus, the bilayer model as described above is characterized completely by the in-layer carrier density n and the inter-layer spacing d.

2.2. Theoretical formalism

For studying the ground-state behaviour of the coupled e–h system, we make use of the dielectric approach, where the density–density linear response function $\chi(q, \omega)$ plays the role of a central quantity. The response function calculation is performed by using the dynamical version of the STLS mean-field approximation. We report here only the central relations of the calculation, and for details, see for instance reference [9]. The intra- and inter-layer response functions are given, respectively, by

$$\chi_{\mathrm{ee}}(Q,\omega) = \chi_{\mathrm{e}}^0(Q,\omega)[1 - \Psi_{\mathrm{hh}}(Q,\omega)\chi_{\mathrm{h}}^0(Q,\omega)]\mathcal{D}^{-1}(Q,\omega), \tag{7}$$

$$\chi_{\mathrm{hh}}(Q,\omega) = \chi_{\mathrm{h}}^0(Q,\omega)[1 - \Psi_{\mathrm{ee}}(Q,\omega)\chi_{\mathrm{e}}^0(Q,\omega)]\mathcal{D}^{-1}(Q,\omega) \tag{8}$$

and

$$\chi_{\mathrm{eh}}(Q,\omega) = \chi_{\mathrm{e}}^0(Q,\omega)\chi_{\mathrm{h}}^0(Q,\omega)\Psi_{\mathrm{eh}}(Q,\omega)\mathcal{D}^{-1}(Q,\omega), \tag{9}$$

where $\chi_l^0(Q,\omega)$ is the density response function of non-interacting carriers in the well l (the so-called Stern function [21]), $\Psi_{ll'}(Q,\omega) = V_{ll'}(Q)[1 - G_{ll'}(Q,\omega)]$, is the effective interaction potential between carriers in the wells l and l', and $\mathcal{D}(Q,\omega)$ is given by

$$\mathcal{D}(Q,\omega) = [1 - \Psi_{ee}(Q,\omega)\chi_e^0(Q,\omega)][1 - \Psi_{hh}(Q,\omega)\chi_h^0(Q,\omega)] - \Psi_{eh}^2(Q,\omega)\chi_e^0(Q,\omega)\chi_h^0(Q,\omega). \tag{10}$$

$G_{ll'}(Q,\omega)$, which is commonly referred to as the LFC factor, describes the effect of short-range correlations among carriers in the wells l and l', and in the dynamical STLS approach it is given by

$$G_{ll'}(Q,\omega) = -\frac{1}{n}\int \frac{\mathrm{d}\mathbf{Q}'}{(2\pi)^2}\frac{\chi_l^0(\mathbf{Q},\mathbf{Q}',\omega)V_{ll'}(Q')}{\chi_l^0(Q,\omega)V_{ll'}(Q)}\left[S_{ll'}(|\mathbf{Q}-\mathbf{Q}'|) - \delta_{ll'}\right]. \tag{11}$$

$\chi_l^0(\mathbf{Q},\mathbf{Q}',\omega)$ is the inhomogeneous non-interacting density response function defined by

$$\chi_l^0(\mathbf{Q},\mathbf{Q}',\omega) = -\frac{2}{\hbar}\int \frac{\mathrm{d}\mathbf{K}}{(2\pi)^2}\frac{f_l^0(\mathbf{K}+\mathbf{Q}'/2) - f_l^0(\mathbf{K}-\mathbf{Q}'/2)}{\omega - \hbar\mathbf{K}\cdot\mathbf{Q}/m_l^* + \mathrm{i}\eta}, \tag{12}$$

where $f_l^0(K)$ is the usual non-interacting Fermi–Dirac distribution function and η is a positive infinitesimal. For $\mathbf{Q}' = \mathbf{Q}$, $\chi_l^0(\mathbf{Q},\mathbf{Q}',\omega)$ reduces to $\chi_l^0(Q,\omega)$. In equation (11), $S_{ll'}(Q)$ is the static density structure factor, which is related, in turn, to the imaginary part of $\chi_{ll'}(Q,\omega)$ in accordance with the fluctuation–dissipation theorem as

$$S_{ll'}(Q) = -\frac{\hbar}{\pi n}\int_0^\infty \mathrm{d}\omega\,\mathrm{Im}\chi_{ll'}(Q,\omega). \tag{13}$$

We note from equations (7)–(9) that the calculation of the density response function $\chi_{ll'}(Q,\omega)$ relies on the knowledge of the LFC factor $G_{ll'}(Q,\omega)$. The LFC factor, in turn, requires the static structure factor $S_{ll'}(Q)$ as input. But, the calculation of $S_{ll'}(Q)$ demands $\mathrm{Im}\chi_{ll'}(Q,\omega)$ (see equation (13)). This implies that the response function calculation involves the self-consistent solution of equations (7)–(9), (11) and (13).

It is appropriate to point out here that the LFC factor is frequency-dependent or dynamic in the quantum STLS approach. This constitutes an important positive feature of the quantum STLS approach over the original STLS method, where the LFC factor is frequency-independent, i.e., static. Further, we note from equation (11) that the quantum STLS inter-layer LFC factor is not symmetric with respect to an interchange of l and l', i.e., $G_{ll'}(Q,\omega) \neq G_{l'l}(Q,\omega)$, for $l \neq l'$. The asymmetry enters directly through the factor $\{\chi_l^0(\mathbf{Q},\mathbf{Q}',\omega)/\chi_l^0(Q,\omega)\}$ in equation (11), for it contains the carrier effective mass m_l^*. An asymmetric inter-layer LFC factor, in turn, will lead to an asymmetric inter-layer density response function $\chi_{ll'}(Q,\omega)$. However, the inter-layer response function $\chi_{ll'}(Q,\omega)$ and hence, the corresponding correlation function $S_{ll'}(Q)$, must remain unchanged under an interchange of l and l'. We surmount this problem of asymmetry by taking the inter-layer LFC factor as the average of $G_{eh}(Q,\omega)$ and $G_{he}(Q,\omega)$. A similar kind of asymmetry problem was encountered by Nafari and Asgari [22] while extending the quantum STLS theory to a multi-sub-band one-dimensional electron gas. Interestingly, there is no such problem of asymmetry with the LFC factor of the conventional STLS approach.

In the next section, we present numerical results for the ground-state properties of a GaAs/GaAlAs based e–h coupled quantum well structure, where we take $m_h^*/m_e^* = 7$.

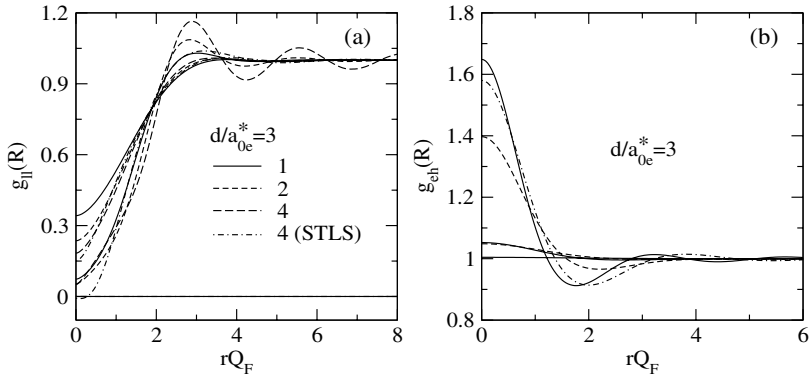

Figure 1. Intra- (in panel (a)) and inter-layer (in panel (b)) pair-correlation functions for the finite width and mass-asymmetric e–h bilayer at $d/a^*_{0e} = 3$ and $r_{se} = 1, 2$ and 4. The STLS results (dash–dot line) are given at $d/a^*_{0e} = 3$ and $r_{se} = 4$. (a) The legends indicate the r_{se} values. At a given r_{se}, the $g_{hh}(R)$ curve originates from the region below the corresponding $g_{ee}(R)$. (b) The results for the finite width and mass-symmetric e–h bilayer are plotted at $r_s = 2$ and 4 by dashed lines. Curves in order of increasing $g_{eh}(R = 0)$ correspond to increasing r_{se}.

3. Results and discussion

3.1. Pair-correlation functions

Before addressing the question on the possibility of transition to a DM phase, we present results for the intra- and inter-layer pair-correlation functions, which constitute rather more basic quantities to describe the behaviour of many-body correlations. The equations (7)–(9), (11) and (13) are solved numerically in a self-consistent manner and a solution is accepted when the convergence in $S_{ll'}(Q)$, at each Q in the grid of Q-points, is better than 0.001%. The pair-correlation function $g_{ll'}(R)$ can then be determined from the inverse Fourier transform of $S_{ll'}(Q)$ as

$$g_{ll'}(R) = 1 + \frac{1}{n}\int \frac{\mathrm{d}\mathbf{Q}}{(2\pi)^2} \mathrm{e}^{\mathrm{i}\mathbf{Q}\cdot\mathbf{R}}[S_{ll'}(Q) - \delta_{ll'}]. \tag{14}$$

We plot, respectively, in figures 1(a) and (b) the intra- and inter-layer correlation functions at different carrier densities r_{se} by keeping the layer spacing fixed at $d/a^*_{0e} = 3$. Here, $r_{se} = 1/(a^*_{0e}\sqrt{n\pi})$ is the electron density parameter, with $a^*_{0e} = \epsilon_0\hbar^2/(m^*_e e^2)$ being the effective Bohr atomic radius for electrons. We notice from figure 1(a) that, for the same number density, the holes are comparatively more strongly correlated as compared to electrons. This difference in the behaviour of correlation functions is on expected lines since, at the same number density, the coupling or the r_s parameter (i.e., the ratio of potential and kinetic energies) for the layer of holes is greater than that for the layer of electrons by a factor of m^*_h/m^*_e, i.e., $r_{sh} = r_{se}(m^*_h/m^*_e)$. Also, the intra- and inter-layer correlations are seen to build up continuously with increasing r_{se} at a given d/a^*_{0e}. To make explicit the dependence of $g_{eh}(R)$ on the mass asymmetry, we have reported in figure 1(b) the corresponding $g_{eh}(R)$ curves by taking $m^*_h/m^*_e = 1$. It may be noted that the heavier holes result in stronger correlations across the layers and the effect becomes even more important with increasing r_{se}. We have also given in figures 1(a) and 1(b) the results of the conventional STLS approach at $r_{se} = 4$ to highlight the importance of the dynamical character of correlations. The STLS $g_{hh}(R)$ is seen to become slightly negative at small R, which is obviously an unphysical result. However, this shortcoming of the STLS approximation is rectified in its dynamical version. Further, it can be seen from figure 1(a) that the difference introduced by the inclusion of the dynamics

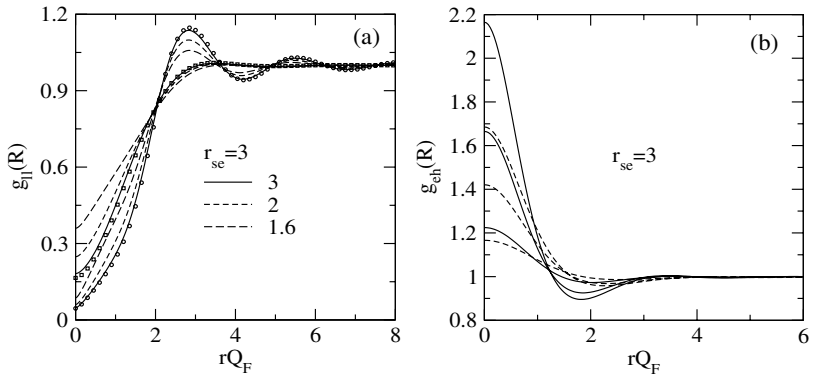

Figure 2. Intra- (in panel (a)) and inter-layer (in panel (b)) pair-correlation functions for the finite width and mass-asymmetric e–h bilayer at $r_{se} = 3$ and $d/a^*_{0e} = 3, 2$ and 1.6. (a) The legends indicate the d/a^*_{0e} values. At a given d/a^*_{0e}, the $g_{hh}(R)$ curve originates from the region below the corresponding $g_{ee}(R)$. The squares (□) and circles (○) represent, respectively, the results of $g(R)$ for the isolated electron and hole layers at $r_{se} = 3$ and $r_{sh} = 21$. (b) Results for the finite width and mass-symmetric e–h bilayer are given at $r_{se} = 3$ and $d/a^*_0 = 3, 2$ and 1.6 by dashed lines. Curves in order of increasing $g_{eh}(R = 0)$ correspond to decreasing d/a^*_{0e}.

of correlations is relatively more pronounced for the layer of holes. This result seems to be compatible with the general observation that the dynamical aspect of correlations should become more pertinent [23, 24] with the increasing value of the coupling parameter.

Figures 2(a) and (b) depict, respectively, the d-dependence of the intra- and inter-layer correlations at a fixed density of $r_{se} = 3$. For ready reference, the results of $g(R)$ for the corresponding isolated layers of electrons and holes are also given in figure 2(a). We note that as the layers are brought closer, the oscillatory structure of both $g_{ee}(R)$ and $g_{hh}(R)$ is found to weaken with respect to their respective single-layer behaviour, while the $g_{eh}(R)$ curves imply a strong build-up of the e–h correlations. The weakening of the oscillatory structure stems from the screening of the intra-layer interaction potential by the carriers of the second layer. As d decreases, the probability of finding a hole exactly opposite to an electron increases, and consequently, the screening of intra-layer correlations grows steadily with the decreasing d. Further, a comparison of our $g_{eh}(R)$ results with the corresponding mass-symmetric case shows (see figure 2(b)) that the mass asymmetry driven growth of e–h correlations becomes increasingly significant, especially at small separation, with the diminishing layer spacing. The comparative picture indicates that the consideration of the mass asymmetry might have serious repercussion on the recent theoretical [8] and simulation [10] predictions of the critical spacing for the stability of an excitonic phase in the e–h bilayer.

In figure 3, we have illustrated the influence of the finite width of layers on the correlations by plotting the intra- and inter-layer correlation functions with and without treating the finite thickness at $r_{se} = 2$ and $d/a^*_{0e} = 1.5$. With the inclusion of the finite width, the in-layer correlations are seen to become weaker, while the correlations between the layers are found to grow somewhat stronger. Apart from these quantitative differences, the correlation functions exhibit a similar dependence on r_{se} and d. The weakening of in-layer correlations is attributed to the softening of the in-layer interaction potential due to the finite width.

3.2. Static density susceptibility and density-modulated phase

In order to examine the stability of the liquid phase against transition into a DM state, we proceed by calculating the liquid-state static (i.e., $\omega = 0$) density susceptibility of the e–h

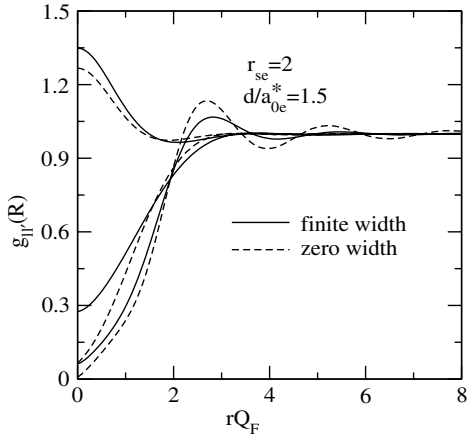

Figure 3. Intra- and inter-layer pair-correlation functions commencing, respectively, in the lower and upper halves of the figure, for the mass-asymmetric e–h bilayer at indicated r_{se} and d/a^*_{0e}, with and without the finite width of layers. The $g_{hh}(R)$ curves originate from the region below the corresponding $g_{ee}(R)$.

system. The phase transition, if any, may appear in the form of a divergence in the static susceptibility at a finite wavevector representing the period of density modulation. For the coupled e–h bilayer, the static density susceptibility is determined by diagonalizing the static density response matrix as

$$\chi_{\pm}(Q,0) = \frac{2}{\chi_e^{-1}(Q,0) + \chi_h^{-1}(Q,0) \pm \left[\{\chi_e^{-1}(Q,0) - \chi_h^{-1}(Q,0)\}^2 + 4\Psi_{eh}^2(Q,0)\right]^{1/2}}, \quad (15)$$

where

$$\chi_l(Q,0) = \frac{\chi_l^0(Q,0)}{1 - \Psi_{ll}(Q,0)\chi_l^0(Q,0)}, \qquad l = \text{e or h}. \quad (16)$$

The + and − signs define, respectively, the in-phase and out-of-phase (π) modes of density modulation in the two layers. As proposed originally by Swierkowski *et al* [25], the in-phase mode can exhibit a singular behaviour at some finite value of Q even if $\chi_e(Q,0)$ and $\chi_h(Q,0)$ are finite at that Q. Based upon this argument, the dynamic STLS theory has predicted [9] for the zero-width and mass-symmetric e–h bilayer, at sufficiently small spacing, the presence of a phase transition from liquid to (i) a WC phase below a critical density ($r_s^c \approx 10$) and (ii) a CDW phase at relatively higher densities ($r_s < 10$). In the following, we investigate in detail the effect of mass asymmetry and finite width of layers on the above prediction of liquid–DM phase transition.

3.2.1. Mass asymmetry effects. To bring out the role of mass asymmetry, we examine the behaviour of $\chi_+(Q,0)$ by first considering the mass asymmetry alone, i.e., we ignore temporarily the finite thickness of layers. The corresponding results of $\chi_+(Q,0)$ are depicted in figures 4(a)–(c) at some selected values of r_{se} and d/a^*_{0e}. We infer from our numerical calculations that $\chi_+(Q,0)$ has a noticeable peak at $Q/Q_F \approx 2.5$ when two layers are sufficiently apart; Q_F is the two-dimensional Fermi wavevector. At a given d/a^*_{0e}, the height of this peak increases quite rapidly with increasing r_{se}, while it becomes somewhat weaker on decreasing d/a^*_{0e} at a fixed r_{se}. However, there begins emerging, at sufficiently small

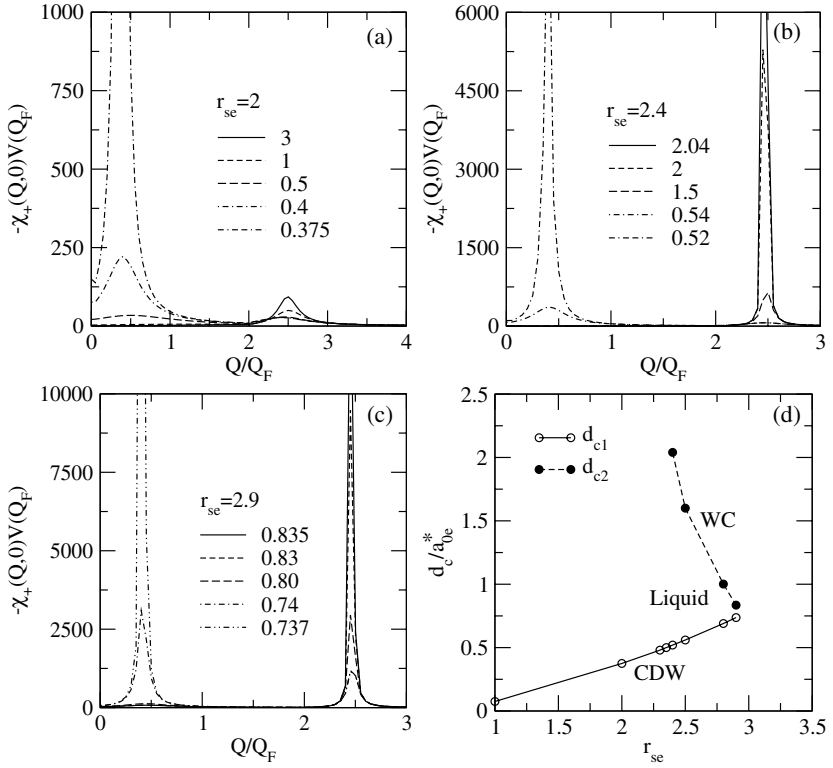

Figure 4. (a)–(c) In-phase component of the static density susceptibility $\chi_+(Q,0)$ for the zero-width and mass-asymmetric e–h bilayer at different r_{se} and d/a^*_{0e}. The legends indicate the values of d/a^*_{0e}. (d) Critical layer spacings d_{c1}/a^*_{0e} (open circles ○) and d_{c2}/a^*_{0e} (solid circles ●) versus r_{se} for the zero-width and mass-asymmetric e–h bilayer. The lines are just a guide for the eye. CDW, liquid and WC refer, respectively, to the stability regions of the charge-density-wave, liquid and Wigner crystal phases.

d/a^*_{0e}, a second peak in $\chi_+(Q,0)$ in the small-Q region, with its strength found to be growing monotonically relative to the $Q/Q_F \approx 2.5$ peak with diminishing d/a^*_{0e}. But, we encounter at each r_{se} a critical spacing (say, d_{c1}) below which it becomes almost impossible to obtain the self-consistent solution of equations (7)–(9), (11) and (13) and, hence the $\chi_+(Q,0)$; for instance, $d_{c1}/a^*_{0e} \approx 0.375$ at $r_{se} = 2$. In figure 4(d), d_{c1}/a^*_{0e} is plotted as a function of r_{se} and it is seen to be an increasing function of r_{se}. Further, we meet with a critical value of r_{se}, namely $r^c_{se} \approx 2.4$, at and above which it is not possible to determine the self-consistent response function not only for $d < d_{c1}$, but also for d higher than a critical spacing d_{c2} ($>d_{c1}$). In this region, i.e., for $r_{se} \geqslant r^c_{se}$ and $d \approx d_{c2}$, the $Q/Q_F \approx 2.5$ peak dominates completely the small-Q peak. d_{c2} is seen to decrease rapidly with the increasing departure of r_{se} from r^c_{se} and it appears to meet d_{c1} approximately at $r_{se} = 3$ (figure 4(d)). In other words, the calculation of the self-consistent response function becomes almost intractable beyond $r_{se} \approx 3$ whatever the value of d/a^*_{0e} is. Although we are not able here to calculate $\chi_+(Q,0)$ for $d < d_{c1}$ when $r_{se} < r^c_{se}$ and for $d_{c2} < d < d_{c1}$ when $r^c_{se} \leqslant r_{se} < 3$, the $Q/Q_F \approx 2.5$ peak appears to diverge for $r_{se} \geqslant r^c_{se}$ and $d \simeq d_{c2}$, while the small-Q peak does so for all r_{se} when $d \simeq d_{c1}$. On the other hand, the out-of-phase component of susceptibility $\chi_-(Q,0)$, as well as $\chi_e(Q,0)$ and $\chi_h(Q,0)$ which comprise the basic ingredients of the susceptibility calculation, always shows

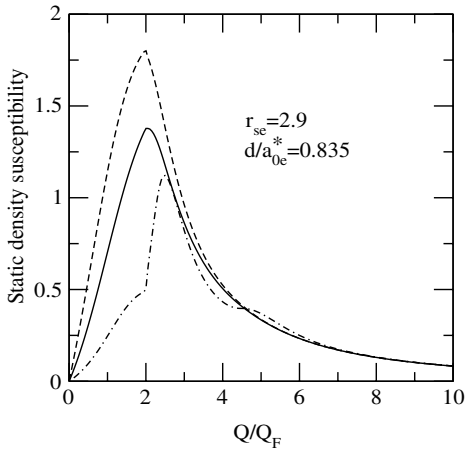

Figure 5. Out-of-phase component of the static density susceptibility $\chi_-(Q,0)$ (solid line ——), $\chi_e(Q,0)$ (dashed line - - - -) and $\chi_h(Q,0)$ (dash–dot line — · —) for the zero-width and mass-asymmetric e–h bilayer at indicated r_{se} and d/a^*_{0e}.

a smooth dependence on Q irrespective of the choice of r_{se} and d. We elucidate this point in figure 5 by plotting these quantities in the critical region, e.g., $r_{se} = 2.9$ and $d/a^*_{0e} = 0.835$; for this choice of parameters, $\chi_+(Q,0)$ nearly diverges at $Q/Q_F \approx 2.5$ as can be noticed from figure 4(c). Thus, it becomes absolutely clear that the large peak in $\chi_+(Q,0)$ originates entirely from its denominator (see equation (15)).

The development of an apparently diverging peak in $\chi_+(Q,0)$ could be interpreted in our theory as an indication for the onset of a phase transition from the liquid to an in-phase DM ground state. The small-Q peak, whose location varies with r_{se}, might indicate an instability of the liquid against a CDW ground state. It is not possible in our theory to draw a firm conclusion about the precise nature of the small-Q DM phase and its recognition as a CDW phase might be just one possibility. On the other hand, the $Q/Q_F \approx 2.5$ peak, whose position lies close to the reciprocal lattice vector of the triangular lattice, could be a precursor for the liquid–WC phase transition. Thus, our theory predicts that the e–h liquid might become unstable against transition into (i) a WC phase below a critical electron density ($r^c_{se} \approx 2.4$) at sufficiently large separation ($d \simeq d_{c2}$) and (ii) a CDW phase always in the adequately close vicinity of layers ($d \simeq d_{c1}$). Consequently, the liquid phase remains stable for d above d_{c1} when $r_{se} < r^c_{se}$ and for $d_{c1} < d < d_{c2}$ when $r^c_{se} \leqslant r_{se} < 3$; see figure 4(d). It is important to note that the critical density for crystallization ($r^c_{se} \approx 2.4$) is increased greatly in the coupled e–h system as compared to the corresponding estimate of the dynamic STLS theory, namely $r^c_{si} \approx 16.45$, for an isolated single electron layer. However, as compared to an isolated hole layer, the crystallization density is slightly decreased, since $r^c_{sh} = r^c_{se}(m^*_h/m^*_e) \approx 16.8$, lies somewhat above r^c_{si}.

Next, we note that for large d the e–h layers should become uncoupled and accordingly, for $r^c_{se} \leqslant r_{se} \leqslant 3$ and $d \gg d_{c2}$, the electrons should be in the liquid phase, while the holes should be in the WC phase, since the corresponding r_{sh} parameter lies above r^c_{si}, the critical crystallization r_s in an isolated layer. A natural question arises: whether the WC phase at d just above d_{c2} is the same as the one realized for $d \gg d_{c2}$ (say, the phase WC-I) or the phase where both the hole and electron layers are in the WC state (say, the phase WC-II). To answer this question, we look into the behaviour of the ratio of the static density modulation in the electron and hole layers, i.e., $[\delta\rho_e(Q,0)/\delta\rho_h(Q,0)]$, for the in-phase eigenmode at $d = d_{c2}$.

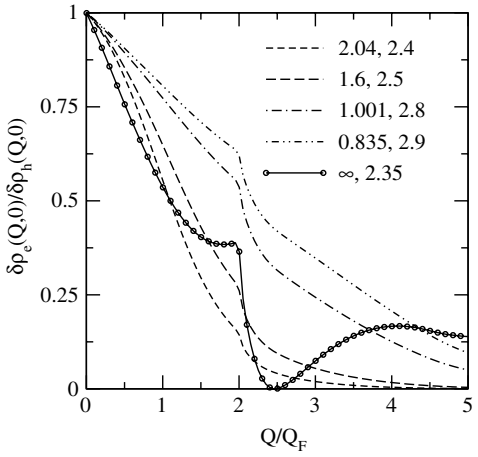

Figure 6. The in-phase component of the ratio of the static density modulation in the electron and hole layers $[\delta\rho_{\rm e}(Q,0)/\delta\rho_{\rm h}(Q,0)]$ for the zero-width and mass-asymmetric e–h bilayer at $d = d_{\rm c2}$ for $2.4 \leqslant r_{\rm se} < 3$. The pair of legends represent the values of $d_{\rm c2}$ and $r_{\rm se}$. The line with circles (O) represents results in the limit $d \to \infty$ at $r_{\rm se} = 2.35$.

If this ratio becomes zero at $Q/Q_{\rm F} \approx 2.5$, it would imply that the e–h bilayer is in the phase WC-I at d just above $d_{\rm c2}$ and it continues in this phase up to $d \to \infty$. On the other hand, a non-zero value of this ratio would imply the stability of the phase WC-II for d just above $d_{\rm c2}$ and hence, the existence of a critical separation $d_{\rm c3}$ ($>d_{\rm c2}$) at which the phase WC-II would transform into the phase WC-I. The ratio $[\delta\rho_{\rm e}(Q,0)/\delta\rho_{\rm h}(Q,0)]$ is plotted in figure 6 for the in-phase eigenmode for different $r_{\rm se}$ satisfying $r_{\rm se}^{\rm c} \leqslant r_{\rm se} < 3$, at their respective values of $d_{\rm c2}$. For ready reference, results are also shown for the uncoupled e–h system (i.e., in the limit $d \to \infty$) by taking $r_{\rm se} = r_{\rm si}^{\rm c}(m_{\rm e}^*/m_{\rm h}^*)(=2.35)$, so that the corresponding $r_{\rm sh}$ equals $r_{\rm si}^{\rm c}$ and the system is in phase WC-I. We notice that the ratio $[\delta\rho_{\rm e}(Q,0)/\delta\rho_{\rm h}(Q,0)]_{Q/Q_{\rm F}\approx 2.5}$ approaches, as per our anticipation, zero in the limit $d \to \infty$ at $r_{\rm se} = 2.35$ and that it takes non-zero finite value at $d = d_{\rm c2}$ for $r_{\rm se}^{\rm c} \leqslant r_{\rm se} < 3$, with its magnitude building up continuously with increasing $r_{\rm se}$. Thus, our results indicate that the electron and hole layers are both in the WC state (i.e., in the phase WC-II) at d just above $d_{\rm c2}$, and therefore imply the existence of a phase boundary between the phases WC-II and WC-I at some critical spacing $d_{\rm c3}$ ($>d_{\rm c2}$). It is not possible to predict $d_{\rm c3}$, since we are not able to obtain the self-consistent LFC factors for $d > d_{\rm c2}$. The layer of strongly correlated holes apparently tends to induce localization in the otherwise less correlated layer of electrons via the attractive e–h correlations. However, on account of mass asymmetry, the localization is relatively less pronounced in the layer of electrons. This point is elaborated in figure 7 by plotting $g_{\rm ee}(R)$, $g_{\rm hh}(R)$ and $g_{\rm eh}(R)$ at $r_{\rm se} = 2.8$ ($>r_{\rm se}^{\rm c}$), and $d = d_{\rm c2}$ ($=1.001a_{0e}^*$) and $d_{\rm c1}$ ($=0.69a_{0e}^*$). Apart from this, one can also note an apparent change in the behaviour of $g_{\rm ee}(R)$ and $g_{\rm hh}(R)$ near transition to the CDW state.

We envisage the following mechanism underlying the above phase transition: as the electron and hole layers are brought in from large distance, the attractive e–h interactions, boosted further by the attractive e–h correlations, tend to compensate for the kinetic-energy cost of crystallization. At the same time, the e–h correlations add to the screening of the intra-layer interaction potential, and thereby act to weaken the in-layer correlations. Both of these effects, which have the same origin but are of opposite nature, grow in their magnitude with decreasing d. Below a critical density ($r_{\rm se}^{\rm c} \approx 2.4$) and at sufficiently large separation ($d \approx d_{\rm c3}$), the localization mechanism seems to win over the screening effects, and consequently supports

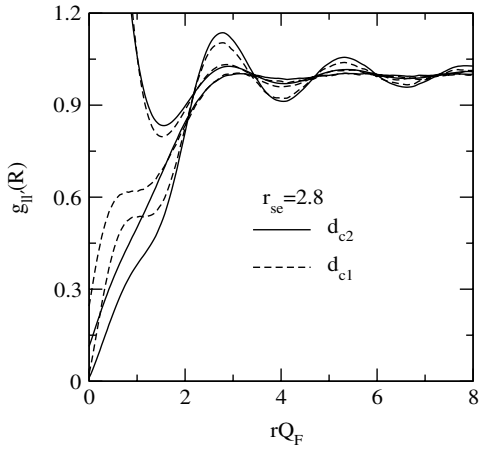

Figure 7. Intra- and inter-layer pair-correlation functions commencing, respectively, in the lower and upper halves of the figure, for the zero-width and mass-asymmetric e–h bilayer at $r_{se} = 2.8$ and $d = d_{c2}$ (=1.001a^*_{0e}) and d_{c1} (=0.69a^*_{0e}). The $g_{hh}(R)$ curves originate from the region below the corresponding $g_{ee}(R)$.

the formation of the coupled WC phase (i.e., the phase WC-II). However, our theory predicts that the coupled WC phase remains stable for $d_{c2} < d < d_{c3}$. This, in turn, suggests that the screening effects start dominating over the e–h correlation-mediated localization for $d < d_{c2}$, and accordingly the liquid phase emerges stable in this region. Decreasing d further causes the liquid to become unstable against a possible CDW ground state for $d < d_{c1}$.

At this stage, it is interesting to compare our above prediction on the DM phase with the corresponding results [9] for the zero-width and mass-symmetric e–h bilayer, where $r_{sh} = r_{se}$ (say, r_s). A cross comparison of results shows that the consideration of the actual effective mass of holes brings about an overall change in the ground state of the e–h bilayer. Among notable points, the crystallization is now predicted at $r^c_{se} \approx 2.4$, a value much lower than the corresponding result, namely $r^c_s \approx 10$, for the mass-symmetric case. Thus, the critical density for Wigner crystallization is enhanced by a factor of about 4. This result constitutes one of the important findings of our present study. Second, it is noted that the build-up of e–h correlations with the diminishing layer spacing ($d \leqslant d_{c2}$) always has a tendency to suppress the $Q/Q_F \approx 2.5$ peak in $\chi_+(Q, 0)$ as compared to the small-Q peak, and therefore the Wigner phase with respect to the CDW phase. At sufficiently small d, these correlations are rather seen to always support the formation of a CDW ground state. This behaviour of the e–h correlations is in contrast with their role in the symmetric e–h system [9], where they are predicted to always support, in the close proximity of layers, the Wigner state for $r_s \geqslant 10$ and the CDW phase for $r_s < 10$; see figure 8(d). Accordingly, the mass-symmetric e–h system exhibits, unlike its mass-asymmetric counterpart, always only one instability at a given r_s, which lies in the region of sufficiently small d (compare figures 4(d) and 8(d)).

It would also be interesting to examine the possibility of the DM ground state by using the conventional STLS method for correlations, for it should reflect directly on the role of the dynamical nature of correlations. We find that the STLS approach predicts, parallel to its application to the mass-symmetric e–h system [7], an instability towards a CDW ground state in the close vicinity of layers. There is no evidence pointing to the formation of a WC state for densities as low as $r_{se} = 10$. Thus, the dynamics of correlations is seen as playing a crucial role in predicting the ground state of the e–h bilayer. The reason underlying different predictions of

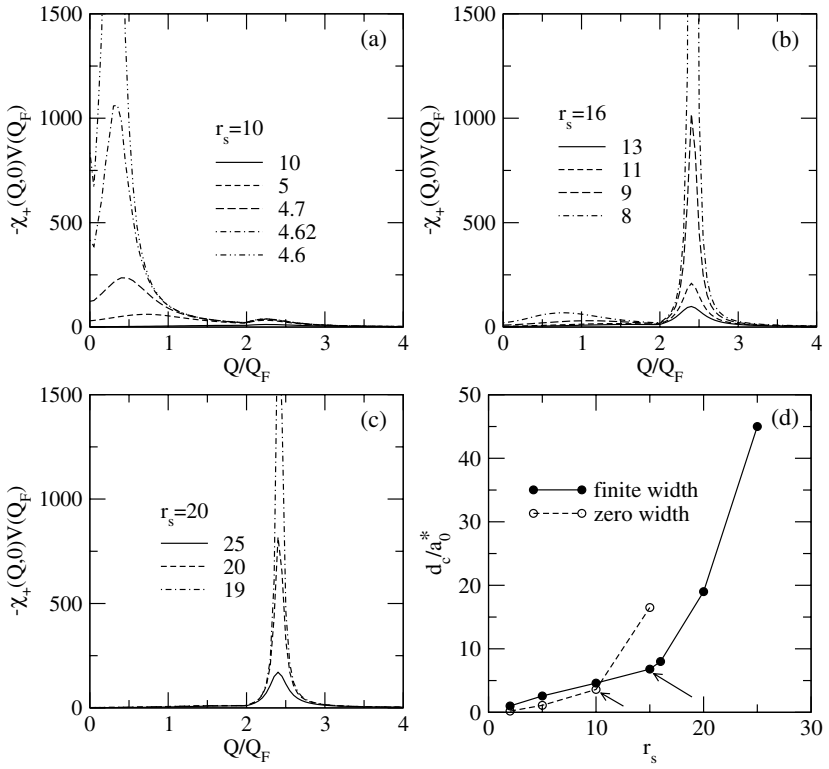

Figure 8. (a)–(c) In-phase component of the static density susceptibility $\chi_+(Q,0)$ for the finite width and mass-symmetric e–h bilayer at different values of r_s and d/a_0^*. The legends indicate the values of d/a_0^*. (d) Critical layer spacing d_c/a_0^* for the transition from the liquid to a DM phase, as a function of r_s for the mass-symmetric e–h bilayer, with (solid circles ●) and without (open circles ○) the finite width of the layers. The arrows point to the critical r_s for crossover from the charge-density-wave instability to the Wigner crystal instability; the lines are just a guide for the eye.

the dynamical and conventional STLS approaches lies in the difference between their respective LFC factors [9].

3.2.2. Finite width effects. For illustrating the impact of the finite width of layers, we now discuss the behaviour of $\chi_+(Q,0)$ for a model e–h system, where layers are treated as of finite width, but mass asymmetry is ignored, i.e., $m_h^*/m_e^* = 1$. For such a system, our calculation reveals that $\chi_+(Q,0)$ exhibits, at the qualitative level, a behaviour similar to that for the corresponding model of zero-width layers [9]. Nevertheless, we report here, for the sake of completeness, the results of $\chi_+(Q,0)$ in figures 8(a)–(c) at some relevant values of r_s and d. To summarize, the e–h liquid can become unstable against a DM phase (of the CDW and WC types) below a critical spacing d_c. The CDW ground state now prevails over the WC phase for r_s approaching 16, and then there occurs a crossover to the WC phase at $r_s \simeq 16$ (figures 8(a)–(c). As compared to an isolated finite thickness layer, the crystallization density is enhanced (by about 40%) due to e–h correlations in the coupled e–h system. For a quick reflection on the effect of finite width, we have reported in figure 8(d) the critical layer spacing d_c/a_0^* for the transition from the liquid to a DM phase, as a function of r_s, with and without the finite width effects. It can be noticed that the inclusion of the finite width results in the lowering of the

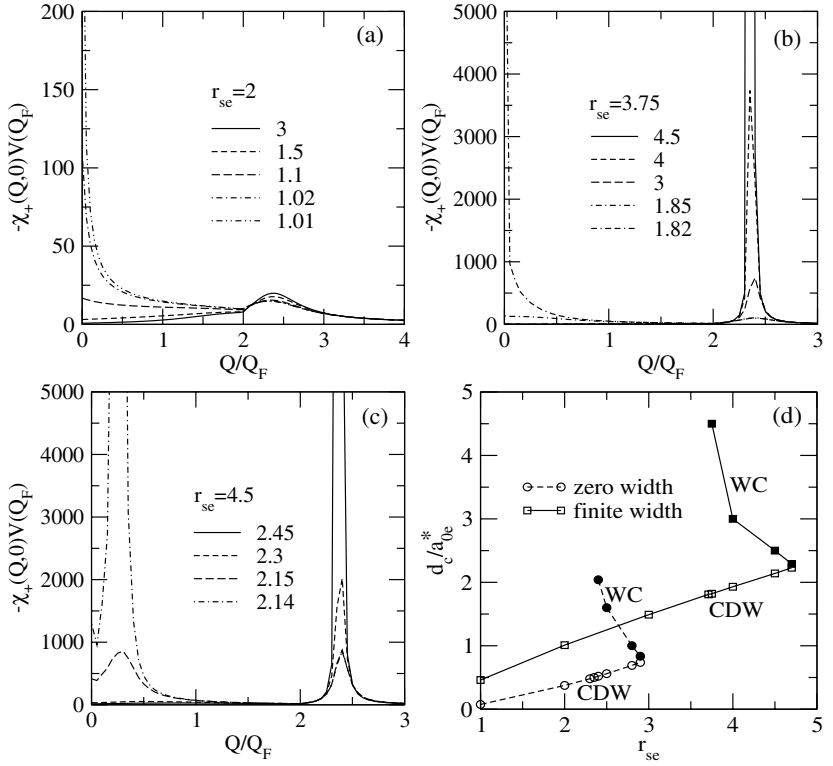

Figure 9. (a)–(c) In-phase component of the static density susceptibility $\chi_+(Q,0)$ for the finite width and mass-asymmetric e–h bilayer at different values of r_{se} and d/a^*_{0e}. The legends indicate the values of d/a^*_{0e}. (d) Critical layer spacings d_{c1}/a^*_{0e} (open symbols) and d_{c2}/a^*_{0e} (filled symbols) as a function of r_{se} for the mass-asymmetric e–h bilayer, with (squares) and without (circles) the finite width of the layers. The lines are just a guide for the eye. CDW and WC refer, respectively, to the stability regions of the charge-density-wave and the Wigner crystal states.

critical density for Wigner crystallization by an appreciable factor of about 1.6. This decrease in crystallization density is attributed to the softening of the intra-layer interaction potential due to the finite thickness, since the softening of interaction is followed by a direct reduction in the strength of intra-layer correlations.

3.2.3. Mass asymmetry and finite width effects. Finally, we compute $\chi_+(Q,0)$ by taking into account both the mass asymmetry and finite width effects. The $\chi_+(Q,0)$ results, seen in conjunction with the calculation that considers only the mass asymmetry, imply that $\chi_+(Q,0)$ does not undergo any qualitative change on inclusion of the finite width of layers. However, there are significant quantitative changes in $\chi_+(Q,0)$ emanating directly from the weakening of intra-layer correlations due to the finite width. As a noticeable change, the Wigner crystallization now occurs at $r^c_{se} \approx 3.75$, which in turn implies that the finite width effects act to lower the critical density for crystallization by a factor of about 1.6. Interestingly, the critical density is lowered by almost the same amount as that for a mass-symmetric e–h bilayer. As in the case of the zero-width e–h system, the crystallization r_s lies slightly above the corresponding value for a finite width isolated hole layer. The results of $\chi_+(Q,0)$ are shown in figures 9(a)–(c) for certain values of r_{se} and d/a^*_{0e}. In figure 9(d), we have displayed the points

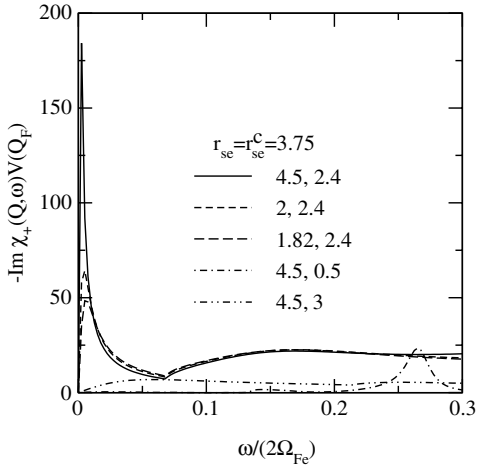

Figure 10. Imaginary part of the in-phase component of the dynamic density susceptibility Im $\chi_+(Q,\omega)$ for the finite width and mass-asymmetric e–h system at $r_{se} = r_{se}^c = 3.75$ and $d/a_{0e}^* = d_{c2}/a_{0e}^*$ (=4.5), d_{c1}/a_{0e}^* (=1.82) and 2, for different values of Q/Q_F. The pair of legends indicate, respectively, the values of d/a_{0e}^* and Q/Q_F. Ω_{Fe} denotes the Fermi frequency for the layer of electrons.

of instability, i.e., d_{c1} and d_{c2}, as a function of r_{se} for the mass-asymmetric e–h bilayer, with and without treating the finite thickness of layers. For d below d_{c1}, the liquid changes into a CDW ground state, whereas for d just above d_{c2} there occurs a liquid–WC phase transition.

3.3. Dynamic excitation spectrum

We noted in the preceding section that the static properties of the e–h system are markedly affected at/near system parameters associated with the liquid–DM phase transition. Keeping this in view, it would be interesting and important to examine the behaviour of the dynamic excitation spectrum of the e–h system in the transition region. One can speculate [26] to find the signs of the above structural transition in the dynamic excitation spectrum. For this purpose, we look into the behaviour of the imaginary part of the density susceptibility $\chi_\pm(Q,\omega)$, which can be obtained from equation (15) on replacing $\omega = 0$ with a variable ω. The only inputs required are the real and imaginary parts of the intra- and inter-layer LFC factors, and these can be determined numerically from equation (11) by using the self-consistent results of $S_{ll'}(Q)$.

In this way, Im $\chi_\pm(Q,\omega)$ is calculated in the entire Q–ω plane over a wide range of r_{se} and d. A careful analysis of results shows that the in-phase mode, i.e., Im $\chi_+(Q,\omega)$, is strongly affected by correlations near the transition region. We demonstrate this point (for the case that treats both the mass asymmetry and finite width of layers) in figure 10 by plotting Im $\chi_+(Q,\omega)$ as a function of ω, keeping Q fixed at a value ($\approx 2.4 Q_F$) equal to the one associated with the WC phase at system parameters in the transition region, namely, $r_{se} = r_{se}^c = 3.75$ and $d/a_{0e}^* = d_{c2}/a_{0e}^*$ (=4.5), d_{c1}/a_{0e}^* (=1.82) and 2. It can be seen that Im $\chi_+(Q,\omega)$ has a noticeable peak at small ω, with its strength increasing rapidly as d approaches the critical spacing (i.e., d_{c2}) for the emergence of the liquid–WC transition. As a notable point, the position of this peak moves towards smaller ω as d is increased towards d_{c2}. Moreover, for $d = d_{c2}$, the position of the peak seems to converge to $\omega = 0$. Though not reported here, we have found a qualitatively similar behaviour of Im $\chi_+(Q,\omega)$ at system parameters appropriate to the liquid–CDW phase transition. Further, if we now vary Q keeping d and r_s

fixed, respectively, at d_{c2} (=4.5a^*_{0e}) and r^c_{se} (=3.75), the small-ω peak is almost suppressed. We illustrate this in figure 10 by reporting Im $\chi_+(Q,\omega)$ for $Q/Q_F = 0.5$ and 3.0 by choosing $r_{se} = r^c_{se} = 3.75$ and $d = d_{c2} = 4.5a^*_{0e}$. The above behaviour of Im $\chi_+(Q,\omega)$ suggests that it costs the system, close to the transition point, very little or nearly zero energy to excite it from the liquid to a DM phase. Consequently, the e–h liquid could become spontaneously unstable with respect to a DM phase for parameters in the transition region. Hence, as envisaged, we detect clear signs of the liquid–DM phase transition in the dynamic excitation spectrum.

4. Summary and concluding remarks

To summarize, we have studied the effect of many-body correlations on the ground-state behaviour of the coupled e–h quantum well structure by taking into account the mass asymmetry and finite thickness of wells. The correlations are treated within the dynamical self-consistent mean-field approximation of Hasegawa and Shimizu. We find that, at the same number density of electrons and holes, the mass asymmetry results in relatively stronger correlation of carriers within the layer of holes as well as across the layers. This change in the behaviour of correlations is seen to have a marked effect on the ground state of the e–h bilayer. As an interesting consequence, the critical density for the onset of Wigner crystallization is enhanced greatly (e.g., by a factor of about 4 for a GaAs/GaAlAs based e–h system) as compared to the corresponding estimate for the mass-symmetric e–h bilayer. However, when compared with an isolated single hole layer, the crystallization density lies slightly on its lower side, and hence implies that the layer of holes compensates partially for the kinetic-energy cost of localization in the otherwise less correlated layer of electrons. Apart from this, we discover a change in the role played by the e–h correlations. These correlations favour the WC phase below a critical density only at sufficiently large layer separation ($d \simeq d_{c2}$). At intermediate separation ($d_{c1} < d < d_{c2}$), the liquid phase represents the stable state, with the liquid, however, becoming unstable against a CDW ground state for $d < d_{c1}$. This behaviour of the e–h correlations is in contrast with their role in the mass-symmetric system, where these correlations are predicted to always support, at sufficiently small separation, the WC phase below a critical density and the CDW phase at higher densities. Further, we have found that the inclusion of the finite thickness of layers amounts to weakening of the intra-layer correlations, and consequently has an effect of lowering the critical density for Wigner crystallization by an appreciable factor of about 1.6.

In conclusion, our study amply demonstrates the role of the mass asymmetry and finite thickness of layers in the study of coupled e–h systems. It particularly emphasizes the importance of the inclusion of these effects into any theoretical or simulation study before drawing a comparison with experiments. It would be interesting to have the computer simulation experiments done on the ground state of a mass-asymmetric coupled e–h bilayer. Our present study could be a stimulant in this direction.

References

[1] For a review, see Rice T M 1977 *Solid State Phys.* **32** 1
Hensel J C, Phillips T G and Thomas G A 1977 *Solid State Phys.* **32** 88
[2] Keldish L V and Kopaev Y V 1965 *Sov. Phys.—Solid State* **6** 2219
Kozlov A N and Maximov L A 1965 *Sov. Phys.—JETP* **21** 790
Keldish L V and Kozlov A N 1968 *Sov. Phys.—JETP* **27** 521
[3] Sivan U, Solomon P M and Shtrikman H 1992 *Phys. Rev. Lett.* **68** 1196
Kane B E *et al* 1994 *Appl. Phys. Lett.* **65** 3266
[4] Lozovik Yu E and Yudson V I 1975 *Sov. JETP Lett.* **22** 274

Lozovik Yu E and Yudson V I 1976 *Solid State Commun.* **19** 391
Lozovik Yu E and Yudson V I 1976 *Sov. Phys.—JETP* **44** 389
[5] Butov L V *et al* 1994 *Phys. Rev. Lett.* **73** 304
Cheng J P *et al* 1995 *Phys. Rev. Lett.* **74** 450
Kono J *et al* 1997 *Phys. Rev.* B **55** 1617
Marlow T P *et al* 1999 *Phys. Rev. Lett.* **82** 2362
Timofeev V B *et al* 2000 *Phys. Rev.* B **61** 8420
[6] Szymanski J, Swierkowski L and Neilson D 1994 *Phys. Rev.* B **50** 11002
[7] Liu L, Swierkowski L, Neilson D and Szymanski J 1996 *Phys. Rev.* B **53** 7923
[8] Liu L, Swierkowski L and Neilson D 1998 *Physica* B **249–251** 594
[9] Moudgil R K, Senatore G and Saini L K 2002 *Phys. Rev.* B **66** 205316
[10] De Palo S, Rapisarda F and Senatore G 2002 *Phys. Rev. Lett.* **88** 206401
[11] Zheng L and MacDonald A H 1994 *Phys. Rev.* B **49** 5522
[12] Alatalo M, Pietiläinen P, Chakraborty T and Salmi M A 1994 *Phys. Rev.* B **49** 8277 and the references given therein
[13] Singwi K S, Tosi M P, Land R H and Sjölander A 1968 *Phys. Rev.* **176** 589
Singwi K S and Tosi M P 1981 *Solid State Physics* vol 36 (New York: Academic) p 177
[14] Tanatar B and Ceperley D M 1989 *Phys. Rev.* B **39** 5005
[15] Hasegawa T and Shimizu M 1975 *J. Phys. Soc. Japan* **38** 965
[16] Alatalo M, Salmi M A, Pietiläinen P and Chakraborty T 1995 *Phys. Rev.* B **52** 7845
[17] Kainth D S, Richards D, Hughes H P, Simmons M Y and Ritchie D A 2000 *J. Phys.: Condens. Matter* **12** 439
[18] Ando T, Fowler A B and Stern F 1982 *Rev. Mod. Phys.* **54** 437
[19] Kainth D S, Richards D, Bhatti A S, Hughes H P, Simmons M Y, Linfield E F and Ritchie D A 1999 *Phys. Rev.* B **59** 2095
[20] Fang F F and Howard W E 1966 *Phys. Rev. Lett.* **16** 797
[21] Stern F 1967 *Phys. Rev. Lett.* **18** 546
[22] Nafari N and Asgari R 2000 *Phys. Rev.* B **62** 16001
[23] Neilson D, Swierkowski L, Sjölander A and Szymanski J 1991 *Phys. Rev.* B **44** 6291
[24] Moudgil R K, Ahluwalia P K and Pathak K N 1995 *Phys. Rev.* B **52** 11945
[25] Swierkowski L, Neilson D and Szymanski J 1991 *Phys. Rev. Lett.* **67** 240
[26] Neilson D, Swierkowski L, Szymanski J and Liu L 1993 *Phys. Rev. Lett.* **71** 4035